Duocarmycins Binding to DNA Investigated by Molecular Simulation †

ARTICLE *in* THE JOURNAL OF PHYSICAL CHEMISTRY B · APRIL 2006

Impact Factor: 3.3 · DOI: 10.1021/jp0548265 · Source: PubMed

3 AUTHORS:

Katrin Spiegel
University of Pennsylvania
20 PUBLICATIONS **621** CITATIONS
SEE PROFILE

Ursula Rothlisberger
École Polytechnique Fédérale de Lausanne
292 PUBLICATIONS **8,521** CITATIONS
SEE PROFILE

Paolo Carloni
Forschungszentrum Jülich
320 PUBLICATIONS **6,088** CITATIONS
SEE PROFILE

Duocarmycins Binding to DNA Investigated by Molecular Simulation†

Katrin Spiegel,‡,||,⊥ Ursula Rothlisberger,§ and Paolo Carloni*,||,⊥

Center for Molecular Modeling, University of Pennsylvania, Philadelphia, Pennsylvania 19104, Laboratory of Computational Chemistry and Biochemistry, EPFL, Ecole Polytechnique Federale de Lausanne, 1015 Ecublens, CH, International School for Advanced Studies, 34100 Trieste, Italy, and DEMOCRITOS, Modeling Center for Research in Atomistic Simulation, INFM, Italy

Received: August 26, 2005; In Final Form: November 15, 2005

Duocarmycins are a potent class of antitumor agents, whose activity arises through their covalent binding to adenine nucleobases of DNA.[1−3] Here, we perform molecular dynamics (MD) and hybrid Car−Parinello QM/MM simulations to investigate aspects of duocarmycin binding to the d(pGpApCpTpApApTpTpGpApC) oligonucleotide. We focus on the derivatives (+)-duocarmycin SA (**DSA**) and (+)-duocarmycin SI (**DSI**), for which structural information of the covalent complex with the oligonucleotide is available, as well as on the related, but less reactive, NBOC−duocarmycin SA (**NBOC−DSA**), interacting with the same oligonucleotide. Comparison is made with adenine alkylation reaction in water performed by the smallest of these compounds (**NBOC−DSA**). The MD calculations suggest that, in noncovalent complexes, (i) drug binding causes a partial dehydration of the minor groove, without inducing a significant conformational changes, and (ii) **DSA** and **DSI** occupy a more favorable position for nucleophilic attack than **NBOC−DSA**, consistently with the lower reactivity of the latter. The QM/MM calculations, which are used to investigate the first step of the alkylation reaction, turn out to provide strongly underestimated free energy barriers. Within these approximations, our calculations suggest that an important ingredient for the experimentally observed DNA catalytic power is the polarization of the drug by the biomolecular scaffold.

II. Introduction

Duocarmycins derivatives (such as those depicted in Figure 1, (+)-**DSA** and (+)-**DSI**) are potent antitumor agents, whose cytotoxic activity arises from their covalent binding to DNA nucleobases, mainly to adenines.[5] These molecules contain a variable number of substituted aromatic ring systems, connected via an amide link to the reactive moiety, a cyclopropyl-indole condensed with a substituted pyrrole ring (ring **A** in Figure 1): the least substituted carbon atom of the cyclopropyl unit (C13 in Figure 1) performs a stereoelectronically controlled addition to the adenine N3 position[6] in a highly selective way (Figure 1).[7]

In the complexes between (+)-**DSA** and (+)-**DSI** with d(pGpApCpTpApApTpTpGpApC)-d(pGpTpCpApApTpTpA*pGpTpC)[1,8] for which the NMR structure is available, the drugs bind selectively to the last nucleobase (A*) of the so-called "A-tract" with guanine as a flanking residue[1]: The A-track contains the A−A, T−T, and A−T (but not the T−A steps) and exhibits a conformation other than that of canonical B-DNA,[9] such as a narrow minor groove, highly negative propeller twists, and a sizable curvature of the double helix.[9−14] The drugs are accommodated in the minor, forming van der Waals interactions between a ring of the molecules (Figure S1) and the sugar nonpolar hydrogens in the minor groove wall and a hydrogen-bond between the C2-carbonyl group and the N2-amino group of G20[2] (Figure S1). The covalent bond is formed between their cyclopropyl unit and N3 of A*. No water molecules are present between the drugs and the DNA minor groove.[2]

DNA acts as a catalyst for this reaction for most duocarmycin derivatives at physiological pH[8,15−17]: **DSA** (Figure 1), which features an indole unit substituted in 5, 6, and 7 positions by three methoxy groups (ring **B**), reacts readily with double-stranded DNA ($k_{obs} = 1.69 \times 10^{-4}$ s^{-1}).[15] **DSI**, in which ring **B** is not substituted, is 20 times less reactive toward DNA than **DSA**. The corresponding reaction in water does not occur at physiological pH, while its $t_{1/2}$ is 177 h at pH 3.[6] The structurally related **NBOC−DSA** compound, in which ring **B** is replaced by a *tert*-butyl group (Figure 1), is 3−4 orders less reactive toward DNA compared to **DSA**.[4]

Several hypotheses regarding the catalytic effect of DNA on the reactivity of the drug have been put forward: (i) Hurley et al. have proposed that a conformational change in the DNA double helix may lead to a more reactive adenine base[18] at the end of the A-tracts. NMR studies reveal particular junction sites at the 3′-end and 5′-end of the A-tract,[9,10] and duocarmycins could specifically target these unusual junctions. Alternatively, duocarmycins by binding to DNA could also trap a particular, more reactive DNA conformation.[19] (ii) Boger et al. have suggested that the higher reactivity of the cyclopropane ring in **DSA** relative to **DSI** is caused by its larger distortion observed in the NMR structures around the amide link (Table 1).[8,15] The distortion is measured by the torsional angles χ_1 (C7−C8−

† Part of the special issue "Michael L. Klein Festschrift".

* To whom correspondence should be addressed. Paolo Carloni, SISSA/ISAS, via Beiut 2-4, 34100 Trieste, Italy. E-mail: carloni@sissa.it.

‡ Unversity of Pennsylvania.

§ Ecole Polytechnique Federale de Lausanne.

|| International School for Advanced Studies.

⊥ Modeling Center for Research in Atomistic Simulation.

10.1021/jp0548265 CCC: $33.50
Published on Web 01/24/2006

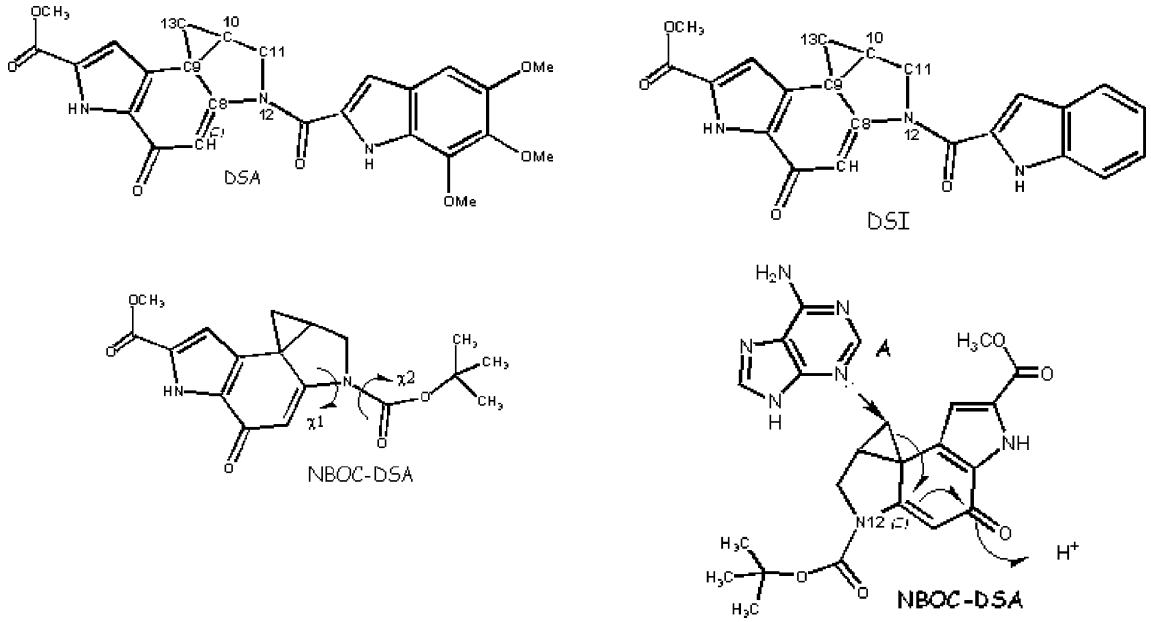

Figure 1. **DSA**, **DSI**, and **NBOC−DSA** duocarmycin derivatives. For **DSA**, ring **A** and ring **B** are indicated and the numeration scheme is provided. For **NBOC−DSA**, the torsional angles around the vinylogous amide bond are displayed and an additional scheme is given displaying the nucleophilic attack.

N12−C16) and χ_2 (C8−N12−C16−O16) (Figure 1) and is believed to decrease the π-electron conjugation and ultimately the stability of the cylcopropyl unit.[4,8] Density functional calculations on a model compound in the gas phase appear not to support this proposal[20] (Table S1, Figure S2), although the effects of the solvent and of the macromolecule are expected to considerably alter these findings in vacuo. (iii) A general acid catalysis or Lewis acid catalysis has also been invoked, in which the drugs are activated by protonation or cation complexation to the O6 group (Figure 1),[21,22] based on the presence of a highly acidic environment around the DNA double helix.[23,24] Measurements of the pH dependency on the reaction rate and consideration of the low pK_a values of the phosphate groups, which could protonate the drugs, argue against this hypothesis.[15,25,26]

Here we investigate some aspects of drug binding and of the reaction mechanism by performing molecular simulations of the complexes between the oligonucleotide and **DSA**, **DSI**, and **NBOC−DSA** (Figure 1). We focus on the neutral form of the drug in this study, which has been suggested by experimental data to be the active form of the drug.[25,26]

First, we carry out MD on the *noncovalent* complexes, that is, before the alkylation reaction, for which no experimental information is available. Our calculations are based on the AMBER force field,[27−29] with drug parameters, which were already used for NMR refinement.[1] Comparison between the calculated and NMR structural properties of the *covalent* adduct establishes the computational procedure used here. Our calculations suggest that the duocarmycin derivatives induce only minor distortions in the DNA scaffold, which argues against a conformational change in DNA responsible for its catalytic activity. Subsequently, we study DNA alkylation reactions of **DSA**, **DSI**, and **NBOC−DSA** with the oligomer by hybrid Car−Parrinello QM/MM simulations.[30] In this approach, the drugs and the alkylated moiety are treated with the BLYP gradient corrected density functional theory,[31,32] whereas the biomolecular frame is treated with the AMBER force field.[28] Comparison is also made with calculations of the hydrolysis reaction of the smallest compound (**NBOC−DSA**). Activation free energies along the N3@adenine−C13@drug reaction coordinate are evaluated using the thermodynamic integration method. The Car−Parrinello QM/MM method in this implementation has been applied to biochemical systems,[30,33−41] showing that it can reproduce relatively well activation free energies. However, the latter for the drug/DNA complexes turns out to be severely underestimated here relative to the experimental value. There are several probable causes of the discrepancy with experiment, including: (i) neglect of part of the entropic cost upon formation of the noncovalent complex,[42] (ii) the deficiency of the BLYP gradient correction in predicting free energy barriers in these systems,[43−46] (iii) the approximation of a single reaction coordinate, which is likely to be an oversimplification,[47,48] other slowly varying degrees of freedom (such as local and global rearrangements of the DNA frame, changes of the electrostatic potential and of the electronic density) may play a non-negligible role,[49] and finally (iv) the ultrashort equilibration time (0.5 ps).[48] Clearly, addressing each of these issues would have greatly increased the computational cost of the simulations, which is already very large. On the other hand, within these large approximations, our calculations provide a description of the structural and electronic properties of the drugs at room temperature in the explicit presence of the DNA frame. In particular, they suggest that the transition state (TS) is characterized by the presence of a negative charge on the drugs efficiently delocalized by their π-electron systems. Finally, they show that the polarization of the biomolecular scaffold on **NBOC−DSA** plays an important role for the DNA catalytic power.

III. Methods

Classical MD. The starting structures of complexes between the oligonucleotide d(pGpApCpTpApApTpTpGpApC)-d(pGpTpCpApApTpTpA*pGpTpC) (**DNA** hereafter) and **DSA** and **DSI** are based on the NMR structures of the covalent complexes cov**DSA·DNA** and cov**DSI·DNA** (1**DSA**[1] and 1**DSI**[8]). The noncovalent adducts **DSA·DNA** and **DSI·DNA** are constructed by removing the covalent bond, closing the cyclopropyl ring,

TABLE 1: MD Simulations

Average Dihedral Angles (in degrees)[a,c]

	DSA NMR	**DSI** NMR	cov**DSA·DNA**	cov**DSI·DNA**
χ_1	22.4(0.7)	14.2(0.6)	14.8(9.4)	15.3(8.7)
χ_2	11.0(0.6)	13.5(0.7)	13.4(10.9)	20.5(8.5)
χ_3	11.4(1.4)	9.7(1.0)	8.4(12.5)	4.7(11.1)

	DSA·DNA	**DSI·DNA**	**NBOC−DSA·DNA**
χ_1	20.9(12.9)	20.2(12.4)	11.7(11.6)
χ_2	14.4(12.1)	16.9(10.6)	−2.3(13.2)
χ_3	9.0(14.3)	6.6(14.4)	

Selected van der Waals Contacts and H-bond Distances (Å)[a,c] between Drugs and **DNA**

	DSA NMR	**DSI** NMR	cov**DSA·DNA**	cov**DSI·DNA**
C25−T18	3.8 (0.3)	3.7 (0.0)	4.0 (0.3)	3.9 (0.3)
C25−T7	3.8 (0.4)	3.7 (0.1)	4.0 (0.3)	3.7 (0.2)
C28−T8	3.9 (0.2)		4.5 (0.3)	
C28−T17	4.0 (0.4)		5.1 (0.6)	
C28−T18	3.9 (0.3)		4.2 (0.4)	
C19−T18	4.2 (0.4)	4.2 (0.0)	4.8 (0.6)	4.1 (0.3)
C19−T7	3.7 (0.3)	4.0 (0.1)	4.1 (0.3)	4.0 (0.3)
C3−A5	4.7 (0.3)	4.8 (0.0)	4.4 (0.4)	4.7 (0.4)
C3−G20	4.0 (0.3)	3.9 (0.0)	4.1 (0.2)	4.1 (0.3)
C14−T21	3.8 (0.4)	3.8 (0.0)	3.9 (0.3)	3.9 (0.4)
H-bond O14	4.1 (1.0)	3.3 (0.8)	5.2 (0.3)	3.9 (1.1)
H-bond O15	3.6 (1.1)	4.6 (0.9)	3.2 (0.3)	5.9 (1.1)

	DSA·DNA	**DSI·DNA**	**NBOC−DSA·DNA**	
C25−T18	3.9 (0.3)	3.9 (0.3)	C19−A6	4.9 (0.9)
C25−T7	4.1 (0.4)	3.9 (0.3)	C19−A19	6.0 (1.7)
C28−T8	4.3 (0.5)	-	C20−A6	5.2 (0.8)
C28−T17	4.2 (0.5)	-	C20-A19	6.6 (1.7)
C28−T18	4.6 (0.6)	-	C21−A6	5.5 (0.8)
C19−T18	4.0 (0.4)	4.1 (0.3)	C21−A19	5.9 (1.4)
C19−T7	3.9 (0.3)	3.9 (0.3)		
C3−A5	5.3 (0.7)	4.8 (0.6)	4.3 (0.7)	
C3−G20	5.5 (0.8)	5.6 (0.7)	5.9 (0.7)	
C14−T21	6.8 (1.5)	6.8 (1.6)	5.2 (1.1)	
H-bond O14	9.6 (1.1)	7.3 (1.0)	6.3 (1.3)	
H-bond O15	7.7 (1.0)	9.0 (1.1)	4.3 (1.3)	

Average root-mean-square Deviations (rmsd's in (Å)/atom)[b,c]

	DNA	drug
cov**DSA·DNA**	1.7 (0.3)	1.8 (0.5)
cov**DSI·DNA**	1.5 (0.2)	1.1 (0.3)
DNA	2.4 (0.5)	-
DSA·DNA	1.9 (0.4)	2.1 (0.6)
DSI·DNA	2.0 (0.5)	2.9 (0.8)
NBOC−DSA·DNA	2.3 (0.5)	5.0 (1.0)

d(C13(drug)−N3(A19)) and *d*(C13(drug)−N3(G20)) Distances (Å)[c]

	DSA·DNA	**DSI·DNA**	**NBOC−DSA·DNA**
C13−N3(A19)	3.6 (0.5)	3.5 (0.4)	4.8 (0.9)
C13−N3(G20)	6.3 (0.5)	5.7 (1.1)	4.1 (0.6)

[a] From covalent drug−**DNA** and noncovalent drug−**DNA** compared to NMR structures.[1,8] [b] For the biomolecular scaffold and drug moieties in the covalent drug−**DNA**, the free oligonucleotide (**DNA**), and noncovalent drug−**DNA** complexes. [c] Standard deviations in parentheses.

and deprotonating the C6−O6 group. Close contacts are removed manually. For the noncovalent **NBOC−DSA·DNA** complex, the drug was fitted on the **DSA·DNA** model and close contacts were again removed manually.

Twenty sodium counterions are added, and the systems are solvated by 4722 (cov**DSA·DNA**), 4809 (cov**DSI·DNA**), 4946 (**DSA·DNA**), 4775 (**DSI·DNA**), and 5013 (**NBOC−DSA·DNA**) water molecules. This leads to a fully solvated system with a water layer of ∼10 Å between the solute and the simulation box, once the system is equilibrated at constant pressure.

For **NBOC−DSA** and adenine in water (**NBOC−DSA·adenine**), the two molecules were placed in a box with 2109 water molecules and the two reactants are oriented similarly as in the drug−DNA complex.

The free **DNA** oligomer is also constructed, using the nucgen module of the AMBER[29] program package. Twenty counterions are added, and the system is solvated with 3903 water molecules.

The AMBER-parm98 force field[28,50] is used for the oligonucleotide, the TIP3P[51] model for water, and the Åqvist parametrization of sodium for the counterions.[52] In the noncovalent complexes, the parameters of **DSA**, **DSI**, and **NBOC−DSA** are adopted from ref 1, except for the charges, which are derived from ESP charges (RESP) as described in the AMBER program package,[29] namely, by optimizing the structures at the B3LYP-6-31G* level of theory. For the noncovalent drugs, the parameters for the O−H bond, and for the cyclopropane ring, are those of the AMBER[28] and gaff[53] force fields, respectively. The AMBER parameters for the *tert*-butyl group of **NBOC−DSA** are adopted.

The charges of the covalent complexes are recalculated both for the drugs and for the attached nucleobase (A19) by the same scheme as described above.

All the drug·**DNA** adducts are minimized by three rounds of steepest descent optimization (5000 steps) using the AMBER7 program,[29] involving (i) the water molecules, (ii) the water and the counterions, and (iii) the entire systems.

Subsequently, the systems undergo MD simulation. The solvent is slowly heated to 300 K at constant volume, keeping the drug·**DNA** adduct frozen. A harmonic position constraint on the drug and DNA is then decreased from a force constant of 2000 kJ/nm^2 to zero in 100 ps of NPT MD.

Periodic boundary conditions are applied, and the electrostatic interactions are calculated with the particle-mesh Ewald method (PME), with a real space cutoff of 12 Å. A time step of 0.001 ps is used. Three separate Nosé−Hoover thermostats[54−56] are applied to the DNA, the drug, and the solvent, which ensure an even temperature distribution throughout the entire system. Constant pressure at 1 atm is controlled through extended-ensemble pressure coupling by a variation of the Parrinello−Rahman method.[57] Bond lengths are constrained using the lincs algorithm, and the translational and rotational motion of the center of mass of the drug·**DNA** adduct is removed every 25 steps of MD. Finally, 10 ns for cov**DSA·DNA**, cov**DSI·DNA**, **DSA·DNA**, **DSI·DNA**, and **NBOC−DSA·DNA**, 6 ns for **DNA**, and 1 ns for **NBOC−DSA·adenine** are collected. In the latter simulation, the distance between the adenine N3 and DSA cyclopropyl carbon is harmonically constrained to a distance of 3.3 Å (K = 5 kcal/(mol·Å^2)). The following properties are calculated (i) root-mean-square deviations (rmsd's),[58] (ii) the number of water molecules H-bonding to atoms of specific chemical groups, calculated by integration of the corresponding radial distribution functions, (iii) occupancy (%) of minor groove binding sites (O2(T/C) and N3(G/A)) by water molecules, calculated as (time H-bond is observed)/(total simulation time)-*100, (iv) drug/**DNA** van der Waals contacts, defined as the minimal distance between any nonpolar **DNA**'s furanose carbon atoms and drug carbon atom, (v) structural parameters of **DNA** (local axis bend, roll and tilt angle, helix twist, minor groove width, propeller twist), which are calculated with the program Curves5.2,[59] excluding the last base pair at each end. The bases are fit to their best planes, and (vi) large scale motions, which are calculated by a covariance analysis along the entire trajectory.[60,61] (The convergence is verified by calculating the overlap between the covariance matrixes of the first and second halves of the trajectories. The cosine content of the normal modes, which turns out to be close to 0, indicates no significant contribution of noise is present in the normal modes.) We focus here on the first three normal modes, which are responsible for 60% of DNA correlated motion.

All the MD calculations are performed with the GROMACS program.[62]

QM/MM Calculations. DSA·DNA, **DSI·DNA**, and **NBOC−DSA·DNA**, **NBOC−DSA·adenine** are divided into two regions.

(i) A QM region, which is treated within the framework of DFT[63] BLYP as implemented in the program CPMD.[63] The basis set consists of plane waves up to an energy cutoff of 70 Ry. Pseudopotentials of the Martins−Trouillers type[64] replace the interactions between the core and the valence electrons. The BLYP functional is used as it is the one far more employed within this approach for biological systems.[31,32] The QM part is treated as an isolated system, and electrostatic interactions between periodic images are decoupled by the scheme of Hockney.[65] The electrostatic interactions between the QM part and the MM part are treated in a hierarchical scheme as described elsewhere.[30,66] A time step of 5 au (0.12 fs) and a fictitious electron mass of 600 au is used. The QM region includes the drugs and the reactive adenine base (A19). The latter is cut at the C1′ carbon, and the valence shell of this last QM atom is saturated by two additional hydrogen atoms (capping hydrogens).[67] The additional capping hydrogens are excluded from the classical Hamiltonian. The QM parts contain 76 (**DSA·DNA**), 64 (**DSI·DNA**), 63 (**NBOC−DSA·DNA**), and 63 (**NBOC−DSA·adenine**) atoms and are placed in an orthorhombic box with box lengths of 23.8 × 14.3 × 21.2 Å^3 (**DSA·DNA**), 23.8 × 20.0 × 15.2 Å^3 (**DSI·DNA**), 18.0 × 14.0 × 18.9 Å^3 (**NBOC−DSA·DNA**), and 19.3 × 14.9 × 20.09 Å^3 (**NBOC−DSA·adenine**), respectively. The overall charge of the QM regions is zero.

(ii) An MM region, which contains the rest of the system, is treated with the effective potentials described in the previous section.[29] The initial structure is an MD snapshot, in which the drug−adenine distance is about 3.3 Å and the counterions are not closer than 5 Å to either the adenine A19 or ring **A** of the drug.

The systems are quenched in the beginning and then relaxed at 0 K. This procedure is repeated several times for the first step along our reaction coordinate, and once for the subsequent steps. The systems are then heated to 300 K. At 300 K, a Nosé−Hoover thermostat is applied to keep the system at constant temperature.[54]

Thermodynamic integration techniques[68,69] are used to calculate the activation free energies of the reactions. We assume that the alkylation reaction can be described by only one reaction coordinate, analogously to refs 30 and 34. An estimate of the free energy of activation is then obtained by integrating the force constant, $f(r)$, along the reaction coordinate[70−72]

$$\Delta F^{\#} = \int \langle f(r) \rangle \, \mathrm{d}r$$

We set this coordinate to be the N3(A19)−C13(drug) distance. At the distances 3.3 Å, 3.0 Å, 2.8 Å, 2.6 Å, 2.4 Å, 2.3 Å, and 2.2 Å, the constraint force is calculated for 1.5 ps. The last 1.0 ps are kept for analysis. The transition state is localized upon the change in the sign of the average constraint. The free energy of activation can be related to k_{cat} through transition state theory

$$k_{cat}(T) = \frac{k_B T}{hc^0} \, \mathrm{e}^{-\Delta F^{\#}/RT}$$

where $\Delta F \sim \Delta G$[73] for our systems. A comparison to the experiment can be done in case of saturation conditions, that is, $k_{obs} \sim k_{cat}$, as it is the case in the systems investigated here. This formula may provide a very approximate value of the catalytic constant because of several problems in estimating $\Delta F^{\#}$ (see Discussion) and because of the inherent strong limitations of this definition for computing rate constants.[47]

The following properties are calculated: (i) Boys orbital centers (BCs) of the fully localized orbitals,[74] calculated on the fly during the QM/MM simulations. BCs are useful to visualize lone pairs and chemical bonds.[74] Here, the polarization index (PI_{AB}) of a chemical bond AB is defined as the ratio of d(A−BC)/d(AB). A PI lower than 0.5 indicates a polarization toward A, a PI larger than 0.5 toward B. A change at the second decimal can be considered significant.[75] (ii) Bond orders[76,77] are calculated on different snapshots for d = 3.0 Å and at the transition state (d = 2.3 Å) and reported for the atoms involved

in bond breaking and bond formation as well as for the aromatic ring involved in the delocalization of the negative charge.

Poisson−Boltzmann Electrostatic Calculations. The nonlinear Poisson−Boltzmann equation is solved iteratively with the program DelPhi[78−80] to calculate the field produced by the DNA scaffold that acts at the position of the drugs examined here. The charges of the drug itself are therefore excluded. The outer dielectric constant of the solvent is set to 80 and the one of DNA to 2.[81] An implicit ionic strength of 0.15 M is added. The average potential is calculated for at least 100 snapshots of the QM/MM trajectory.

All the calculations were carried out on an IBM Linux Cluster 1350 featuring Intel Xeon PentiumIV 3.055GHz processors.

IV. Results

Here, we describe the MD structures of the noncovalent complexes between the oligomer (**DNA** hereafter) and **DSA**, **DSI**, or **NBOC−DSA**. Our computational setup for the MD simulations is established by reference calculations on the covalent **DSA·DNA** and **DSI·DNA** adducts, for which the 3D structure has been determined.[1] The structures of the biomolecular scaffold are compared with those obtained with an MD simulation of the oligomer in the free state. Next, we discuss the alkylation reaction of **DSA**, **DSI**, and **NBOC−DSA** with DNA based on our constrained QM/MM simulations. For the smallest drug, **NBOC−DSA**, comparison is made for the correspondent reaction with adenine in water.

Classical MD Simulations. We focus on the complexes between the drugs and **DNA** in aqueous solution. The drugs are covalently (cov**DSA·DNA**, cov**DSI·DNA**) or noncovalently bound (**DSA·DNA**, **DSI·DNA,** and **NBOC−DSA·DNA**). The systems are built based on the NMR structures of the covalent complexes (Figure S1)[1]. Comparison is also made with the structure of the oligomer (**DNA**) featuring the canonical B-DNA conformation.

Validation of the Computational Setup: MD on covDSA·DNA, covDSI·DNA. Since the force field for the drug is nonstandard (see Methods), MD simulations on cov**DSA·DNA**, cov**DSI·DNA** are performed and compared with experimental data. In addition, these calculations provide insights on the conformational fluctuations of these adducts.

Our MD structures turn out to rearrange only very slightly from the initial NMR structures: (i) The rmsd's (all atoms) of the DNA moiety fluctuate around 1.5−1.7 Å/atom after 0.5 ns (Table 1); those of the drugs fluctuate around 1.8 Å/atom. (ii) The minor groove width is similar and smaller than that of canonical B-DNA[1,8] (Figure 2). (iii) The propeller twists are similar and largely negative at the A-tract (Figure 2). (iv) The overall DNA curvature ranges from 15° to 17° mostly caused by a local axis bend at the end of the A-tract. The largest local axis bend for **DSI−DNA** is found at the T4−A5 step for both MD and NMR structures, whereas that of **DSA−DNA** is located at the T4−A5 step in the MD structure and at the A5−A6 step in the NMR structure. (v) The twist angles at the T4−A5 step are similar and lower than those of canonical B-DNA (Figure 2). (vi) The van der Waals and H-bond contacts are similar, although in the NMR structure, the contact distances are in general shorter (by 0.2 Å, Table 1). This may be the reason for the difference seen for the tilt angle at the alkylation site (Figure 2). The torsional angles around C7−C8−N12−C16 (χ_1) and around C8−N12−C16−O16 (χ_2), which measure the degree of distortion of the amide link (Figure 1), are fairly similar to the NMR values although χ_1 differs upon passing from **DSA** to **DSI** only in the NMR structure (Table 1).

We conclude that, within the limitations of the relatively short time scale investigated, our computational setup is able to reproduce fairly well the structural properties of the NMR structure.

MD Simulation of DNA. The rmsd between the final MD structure of DNA and the initial structure is as large as 2.5 Å, pointing to the well-known differences[82] between the B-conformation and the conformation of A-tracts in solution. In particular for the A-Tract, the MD structure exhibits: (i) a narrower minor groove, with the narrowest value at the A6 site (4.5 vs 5.7 Å for standard B-DNA),[82] (ii) more negative propeller twists in the A-tract (−20° vs −11° in B-DNA), and (iii) larger local axis bends and roll angles at the end of the A-tract. In B-DNA, both local axis bend and roll angle are ideally 0°.[82] The backbone torsional angles are instead similar to those in canonical B-DNA (Table S4).[82]

MD Simulations of DSA·DNA, DSI·DNA, and NBOC−DSA·DNA. As expected, the noncovalent **DSA·DNA** and **DSI·DNA** adducts, constructed from the covalent NMR structures, exhibit slightly larger rmsd's from the initial models than those of the covalent complexes (Table 1). The initial MD structure of **NBOC−DSA·DNA**, for which no experimental structure is available, is derived from the covalent **DSA·DNA** complex. The *tert*-butyl unit, which replaces the indole unit of **DSA**, is bulky and penetrates less into the minor groove. Therefore, it is not surprising that the rmsd of **NBOC−DSA·DNA** is higher than that of **DSA·DNA** or **DSI·DNA** (Table 1).

The mutual rmsd's between the noncovalent drug−**DNA** complexes and **DNA** are small, ranging from 0.5 to 0.7 Å. These structures exhibit: (i) A narrow minor groove with the narrowest value at the A6 site, (ii) high negative propeller twists in the A-tract, (iii) increased local axis bend and roll angles at the ends of the A-tract, and (iv) a low helix twist at the T4−A5 step.

The latter is also observed in the covalent drug−**DNA** complexes, thus this seems to be an inherent feature of the sequence studied here and not a distortion due to the drug as proposed in ref 1.

The overall DNA curvature ranges from 18° to 29°, similar to that of **DNA** and higher than that of the covalent drug−**DNA** complexes (Table S2/3). The local axis bends at the T4−A5 step are slightly larger than in **DNA** (by 1−2°, Figure 2) and exhibit larger fluctuations (see standard deviations, Table S2/3). The roll angles are positive at the end of the A-tracts (T4−A5, T8−G9) and account for most of the local axis bends. All other base steps are characterized by a roll angle close to 0°. The propeller twists are larger at the A5−T18 base pair than in **DNA** (Figure 2) in all three drug−**DNA** complexes.

The fluctuations of these quantities at the drug-binding site are slightly larger compared to the ones of **DNA** and much larger than those of the covalent complexes (Table S2/3). The minor groove widths of **DSA·DNA** and **DSI·DNA** are very similar to **DNA** and wider at the T4 and A5 step with respect to the covalent drug−**DNA** adducts (Figure 2). On the other hand, the minor groove of **NBOC−DSA·DNA** at the alkylation site and at the two subsequent steps is wider than those of **DSA·DNA**, **DSI·DNA**, and **DNA**.

We conclude that the overall oligonucleotide structure is only slightly perturbed by the presence of the drugs as already pointed out in ref 1.

We now investigate the mode of binding of the three drugs. The rmsd's, calculated by fitting only the DNA scaffold, suggest that **NBOC−DSA** rearranges significantly in the minor groove, whereas **DSA** and **DSI** remain close to their initial positions

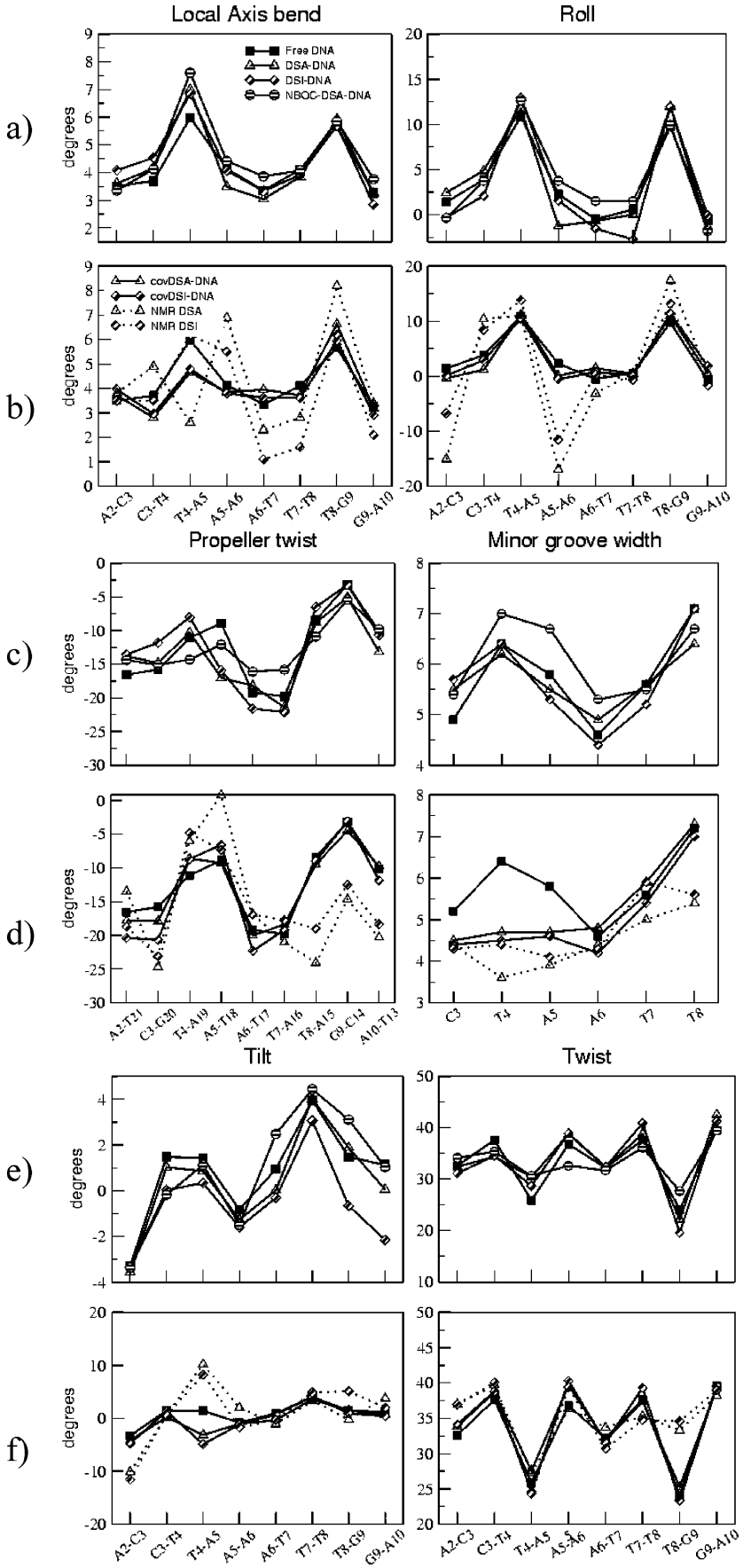

Figure 2. MD simulations: selected helical parameters for d(pGpApCpTpApApTpTpGpApC) (DNA). Both those of **DSA·DNA**, **DSI·DNA**, and **NBOC**−**DSA·DNA** MD structures (a, c, and f) as well as of cov**DSA·DNA** and cov**DSI·DNA** NMR and MD structures (b,d, and e) are reported. Comparison with those of the average **DNA** MD structure is made: black squares, **DNA**; empty triangles, **DSA**−**DNA**; diamonds with diagonal stripes, **DSI**−**DNA**; circles with horizontal stripes, **NBOC·DNA**; Dashed lines, NMR experiment. The parameters have been averaged over 10 ns trajectories.

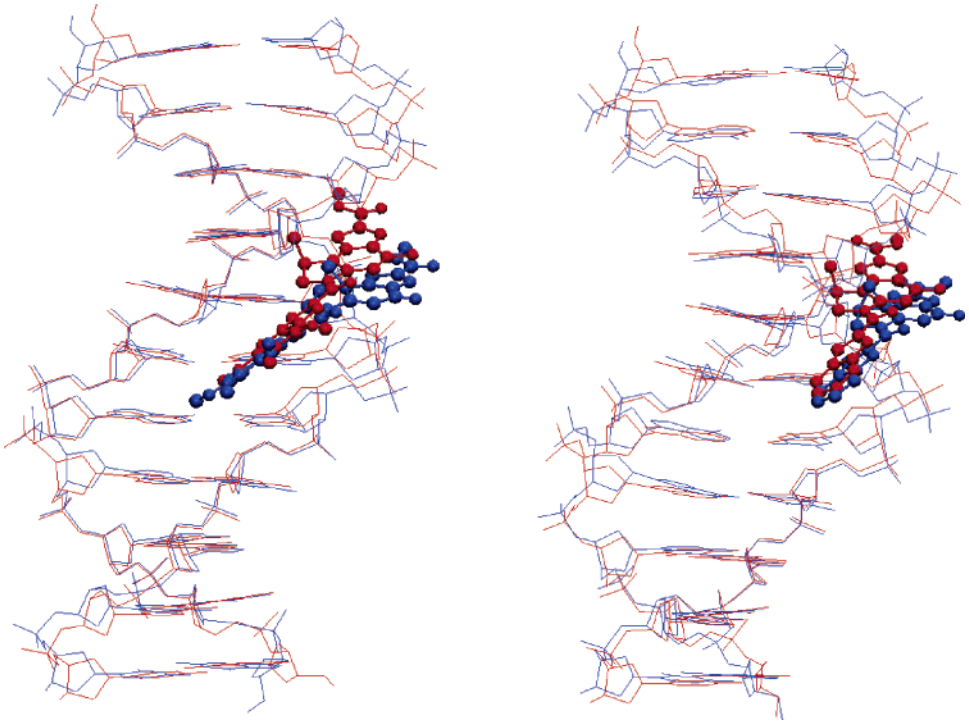

Figure 3. MD simulations: structure of the drug/DNA adducts. Superposition of MD covalent (red) and noncovalent (blue) **DNA** adducts with **DSA** (A) and **DSI** (B). In both complexes, ring **B** remains almost in the same position and ring **A** experiences significant rearrangements in the minor groove. The fit has been performed only on the DNA residues. The rmsd's between the DNA scaffolds are in both cases 1.2 Å.

(Table 1). For **DSA·DNA** and **DSI·DNA**, the distance between the reactants (atoms C13(drug) and N3(A19), *d* hereafter) fluctuates between 3 and 4 Å, leading to a reactive complex between the drug and DNA (Table 1, Figure S3). Instead, the corresponding distance in **NBOC−DSA·DNA** fluctuates between 3 and 9 Å, and *d*(C13(drug)−N3(G20)) oscillates between 3 and 6.0 Å (Table 1, Figure S3). Thus, this guanine nucleobase could be an alternative alkylation site for **NBOC−DSA**. So far, alkylation at guanine sites has only been observed for a structurally related compound[83] and not for **NBOC−DSA** itself.

Ring **B** of **DSA** and **DSI** forms basically the same van der Waals interactions as the covalent complexes but is slightly shifted to the 5′-end of the modified strand (Table 1, Figure 3). The C28 methoxy group of **DSA** forms additional contacts with the minor groove. **NBOC−DSA**, in which ring **B** is substituted by a *tert*-butyl group, forms less hydrophobic contacts with **DNA**. The three methyl groups are equivalent and in contact with the sugar rings of A19 and A6 (Table 1). Ring **A** of **DSA** and **DSI** is located further away from the alkylation site and forms less van der Waals contacts to the minor groove than in the correspondent covalent adducts. The C2−carbomethoxy−N2(G20) H-bond[2] is mediated by one water molecule. Ring **A** of **NBOC−DSA** forms tighter hydrophobic contacts than the other two drugs and a direct H-bond for most of the simulated time.

Comparison Among the Models. In this section, we compare selected features of the systems investigated by MD simulations.

In the drug−**DNA** complexes, the hydrophobic contacts between ring **B** and the minor groove are similar; those between ring **A** and **DNA** are shorter in the covalent complexes. A superposition of covalent and noncovalent complexes is presented in Figure 3. The only hydrogen bond present between G20 and the methyl-carboxy group is direct in the covalent complexes whereas it is mediated by one water molecule in the noncovalent complexes. The two carbonyl groups are solvent exposed in all systems (Figure S1).

The χ_1 and χ_2 torsion angles of **DSA** and **DSI** (Figure 1) are very similar and larger than those of **NBOC−DSA** (Table 1). Furthermore, they are larger and fluctuate more than those of the corresponding covalent drug**·DNA** complexes (Table 1). Thus, **DSI** and **DSA** are more distorted and flexible in the free state than when bound to DNA.

We have observed that spatial fluctuations of the noncovalent complexes are slightly larger than those of the free nucleotide and considerably larger compared to those of the covalent complexes. These findings are substantiated by an analysis of the large-scale motions. In fact, the latter are characterized by changes in the minor groove width and the DNA curvature (Figure S4). The minor grooves open up and close again. The widths and the curvature of the noncovalent complexes are fairly similar to those of **DNA** and vary by as much as 3 Å and 15°, respectively (Figure S4). This further confirms that the drug does not largely affect the structure and dynamics of the DNA scaffold. In the covalent adducts, the variation in minor groove width is much smaller (Δ width, 0.2−0.5 Å), whereas DNA curvature still varies considerably (Δ curvature, 14°). The latter is however due to enhanced fluctuation of the local axis bend at the T8−G9 step, which is outside the drug-binding site. Thus, the formation of the covalent bonds leads to a stiffening of the drug-binding site (Figure 2, Table S2/3, Figure S4/5).

We close this section by investigating the hydration of the drug-binding site. The minor groove of the MD structure of **DNA** is fully hydrated and the water molecules form the typical spine of hydration (Figure 4).[12,84] The presence of the drug leads to removal of several ordered water molecules in the minor groove with respect to **DNA** (Figure 4). In **DSA·DNA** and **DSI·DNA**, A6 and T18 are fully dehydrated and A19 and A5 are partially dehydrated as seen in the water occupancy (see Methods). In **NBOC−DSA·DNA**, G20, T4, A19, and A5 have low water occupancy again showing that ring **A** of **NBOC−DSA** is more tightly bound to the minor groove than **DSA** and **DSI**.

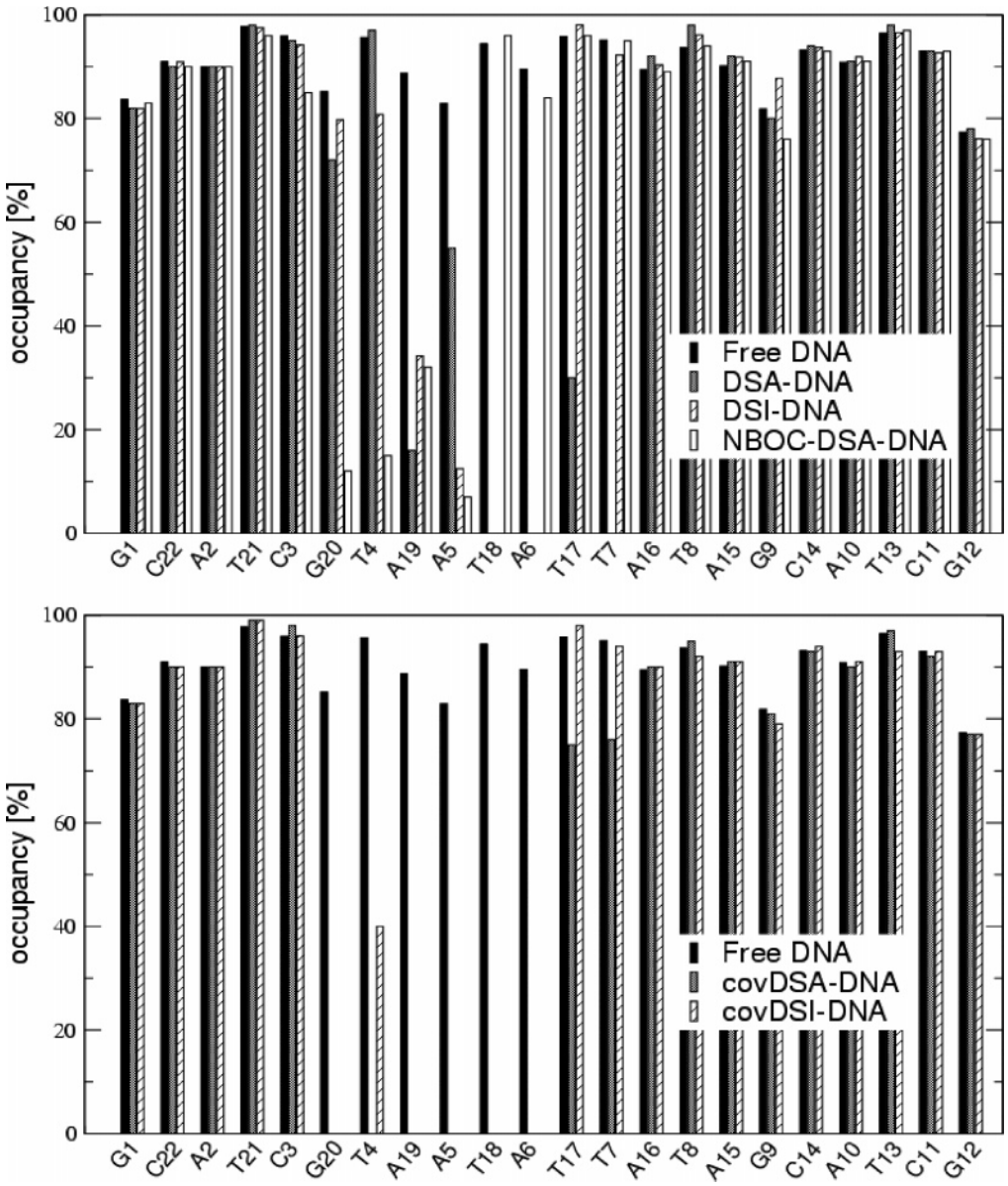

Figure 4. MD simulations: water occupancy in the minor groove of the drug/DNA adducts. The occupancies (see Methods) of the noncovalent (upper panel) and covalent (lower panel) drug−**DNA** MD adducts are shown. Comparison with the average **DNA** MD structure is made.

Covalent binding leads to further removal of water molecules from the minor groove in agreement with ref 1. In cov-**DSA·DNA**, G20, T4, A19, A5, A6, and T18 are fully dehydrated. In cov-**DSI·DNA**, the same sites are also fully dehydrated with the exception of T4, which has some residual water occupancy at this site (Figure 4).

QM/MM Calculations. Reactions of DSA, DSI, and NBOC−DSA with DNA. These reactions have been shown to occur via an S_N2 mechanism[6,85] with the rate-limiting step being the attack of the N3 atom of A19 on the least substituted carbon atom of the cyclopropyl unit (C13). Simultaneously, the C9−C13 bond is elongated and eventually broken, whereas the other two bonds in the cyclopropyl ring, *d*(C9−C10) and *d*(C10−C13), get shorter. In the second step, which is faster,[6] the carbonyl oxygen in the O6 position is protonated.

The reactions here are investigated by QM/MM techniques, calculating activation free energies using thermodynamic integration along a reaction coordinate as in refs 30, 34, and 43. At selected steps along the reaction coordinate, structural and electronic properties (polarization index (PI), bond orders, and ESP partial atomic charges[86]) are monitored. In particular, (i) changes of bond orders on the N3−C13 and C9−C13 bonds help characterize the transition states as they are involved in bond formation and bond breaking, respectively. In general, an early transition state, which resembles more the reactant than the products has a lower activation barrier than a late transition state, which more resembles the products. (ii) Changes of bond orders along the O14−C14−N12−C8 bonds give insights on the role of vinylogous conjugation postulated in ref 8: a decrease of the double bond character of the C8−N12 bond and a strengthening of the carbonyl double bond would indicate a rupture of the vinylogous conjugation. (iii) Finally, the change of the aromatic conjugation in the six-membered ring of the indole unit is followed in terms of bond lengths and bond orders and reflects the increasing π-conjugation as all the bonds involved are becoming similar.

The reaction coordinate for the thermodynamic interaction is here set to be the *d*(N3(A)−C13(drug)) distance (*d* hereafter). We thus make the approximation of a monodimensional reaction coordinate as already made for a variety of biochemical reactions.[30,34] Our initial structures are MD conformations in which $d = 3.3$ Å. These are frequently encountered in the MD

TABLE 2: QM/MM Simulations

D-RESP Charges, Bond Lengths, and Angles for Selected Atoms[a]

	DSA·DNA			
N3−C13 constrained distance	3.0	2.6	2.4	2.3
D-RESP (N3)	−0.035	−0.015	0.019	0.032
d(C9−C13)	1.590 (0.026)	1.660 (0.050)	1.816 (0.104)	2.057 (0.095)
d(C9−C10)	1.558 (0.019)	1.545 (0.020)	1.526 (0.012)	1.520 (0.011)
d(C10−C13)	1.467 (0.011)	1.461 (0.010)	1.464 (0.011)	1.475 (0.014)
d(C9−C8)	1.467 (0.009)	1.461 (0.011)	1.443 (0.012)	1.422 (0.009)
d(C8−C7)	1.379 (0.008)	1.385 (0.010)	1.388 (0.009)	1.399 (0.010)
d(C7−C6)	1.444 (0.011)	1.439 (0.013)	1.441 (0.012)	1.430 (0.012)
d(C6−C5)	1.446 (0.011)	1.441 (0.012)	1.440 (0.012)	1.437 (0.012)
d(C5−C4)	1.412 (0.009)	1.411 (0.008)	1.416 (0.010)	1.422 (0.009)
d(C9−C4)	1.458 (0.011)	1.454 (0.012)	1.440 (0.013)	1.425 (0.011)
∠N3−C13−C9	157 (5)	161 (5)	161 (7)	160 (5)
∠C13−C9−C10	56 (1)	54 (1)	51 (2)	46 (2)
∠C10−C13−C9	61 (1)	59 (2)	54 (3)	48 (3)
∠C13−C10−C9	63 (1)	67 (3)	75 (5)	87 (5)
	DSI·DNA			
N3−C13 constrained distance	3.0	2.6	2.4	2.3
D-RESP (N3)	−0.014	0.009	0.044	0.030
d(C9−C13)	1.592 (0.033)	1.645 (0.041)	1.786 (0.112)	1.971 (0.109)
d(C9−C10)	1.541 (0.018)	1.540 (0.017)	1.532 (0.013)	1.520 (0.009)
d(C10−C13)	1.480 (0.014)	1.473 (0.010)	1.466 (0.007)	1.474 (0.015)
d(C9−C8)	1.474 (0.009)	1.464 (0.011)	1.447 (0.009)	1.433 (0.009)
d(C8−C7)	1.383 (0.007)	1.383 (0.010)	1.388 (0.007)	1.393 (0.008)
d(C7−C6)	1.441 (0.013)	1.447 (0.012)	1.443 (0.009)	1.431 (0.008)
d(C6−C5)	1.444 (0.011)	1.449 (0.014)	1.443 (0.009)	1.440 (0.009)
d(C5−C4)	1.407 (0.008)	1.412 (0.010)	1.414 (0.008)	1.420 (0.006)
d(C9−C4)	1.458 (0.013)	1.455 (0.014)	1.440 (0.009)	1.432 (0.010)
∠N3−C13−C9	158 (7)	171 (5)	169 (5)	164 (4)
∠C13−C9−C10	56 (1)	55 (1)	52 (2)	48 (2)
∠C10−C13−C9	60 (1)	59 (1)	55 (3)	50 (3)
∠C13−C10−C9	64 (2)	66 (2)	73 (6)	82 (5)
	NBOC−DSA·DNA			
N3−C13 constrained distance	3.0	2.6	2.4	2.3
D-RESP(N3)	−0.056	−0.055	−0.007	0.018
d(C9−C13)	1.591 (0.032)	1.626 (0.032)	1.791 (0.085)	1.990 (0.105)
d(C9−C10)	1.573 (0.022)	1.559 (0.021)	1.536 (0.015)	1.529 (0.009)
d(C10−C13)	1.470 (0.009)	1.462 (0.012)	1.456 (0.006)	1.468 (0.012)
d(C9−C8)	1.447 (0.011)	1.464 (0.011)	1.439 (0.015)	1.424 (0.007)
d(C8−C7)	1.374 (0.008)	1.377 (0.008)	1.388 (0.008)	1.395 (0.005)
d(C7−C6)	1.444 (0.011)	1.439 (0.011)	1.431 (0.010)	1.427 (0.008)
d(C6−C5)	1.451 (0.013)	1.446 (0.012)	1.441 (0.010)	1.439 (0.009)
d(C5−C4)	1.409 (0.008)	1.411 (0.007)	1.416 (0.009)	1.421 (0.006)
d(C9−C4)	1.466 (0.013)	1.462 (0.012)	1.443 (0.010)	1.433 (0.009)
∠N3−C13−C9	166 (6)	157 (4)	156 (4)	156 (4)
∠C13−C9−C10	56 (1)	55 (1)	51 (2)	47 (2)
∠C10−C13−C9	62 (1)	60 (1)	55 (3)	50 (3)
∠C13−C10−C9	62 (1)	65 (2)	74 (4)	83 (5)
	NBOC−DSA·adenine			
N3−C13 constrained distance	3.0	2.6	2.4	2.3
D-RESP (N3)	−0.270	−0.229	−0.313	−0.154
d(C9−C13)	1.580 (036)	1.626 (0.036)	1.768 (0.087)	2.168 (0.147)
d(C9−C10)	1.559 (0.027)	1.554 (0.022)	1.535 (0.020)	1.524 (0.012)
d(C10−C13)	1.478 (0.012)	1.467 (0.009)	1.466 (0.011)	1.486 (0.014)
d(C9−C8)	1.477 (0.015)	1.466 (0.010)	1.449 (0.015)	1.412 (0.008)
d(C8−C7)	1.379 (0.009)	1.377 (0.009)	1.388 (0.011)	1.407 (0.008)
d(C7−C6)	1.441 (0.012)	1.440 (0.011)	1.441 (0.014)	1.426 (0.009)
d(C6−C5)	1.447 (0.020)	1.446 (0.010)	1.444 (0.015)	1.432 (0.009)
d(C5−C4)	1.408 (0.010)	1.412 (0.007)	1.413 (0.010)	1.423 (0.009)
d(C9−C4)	1.464 (0.017)	1.461 (0.010)	1.447 (0.015)	1.421 (0.010)
∠N3−C13−C9	165 (9)	155 (7)	153 (6)	146 (6)
∠C13−C9−C10	56 (1)	55 (1)	52 (2)	43 (3)
∠C10−C13−C9	61 (2)	60 (2)	56 (3)	45 (4)
∠C13−C10−C9	63 (2)	65 (2)	72 (4)	92 (7)

Activation Free Energies (kcal/mol)

	DSA·DNA	**DSI·DNA**	**NBOC−DSA·DNA**	**NBOC−DSA·adenine**
$\Delta G^{\#}$ theor.	10.5 ± 3.4	13.8 ± 3.6	12.1 ± 2.4	16.1 ± 4.0
$\Delta G^{\#}$ exp.	22.7	24.5	26.8−28.2	

TABLE 2 (Continued)

Bond Orders at N−C13 Constrained Distance of 3.0 Å (left, normal) and at the Transition State, Constrained Distance of 2.3 Å (right, italic)

bond	**DSA·DNA**	**DSI·DNA**	**NBOC−DSA·DNA**	**NBOC−DSA·adenine**
		Reactive Bonds		
N3−C13	0.008 *0.221*	0.019 *0.208*	0.009 *0.221*	0.009 *0.327*
C9−C13	0.809 *0.410*	0.803 *0.411*	0.814 *0.395*	0.815 *0.240*
		Six-Membered Ring		
C9−C8	1.061 *1.201*	1.051 *1.193*	1.065 *1.212*	1.028 *1.279*
C8−C7	1.502 *1.412*	1.456 *1.392*	1.460 *1.212*	1.463 *1.329*
C7−C6	1.133 *1.192*	1.181 *1.218*	1.177 *1.221*	1.152 *1.268*
C6−C5	1.076 *1.128*	1.101 *1.128*	1.082 *1.126*	1.083 *1.153*
C5−C4	1.291 *1.257*	1.302 *1.259*	1.298 *1.257*	1.286 *1.241*
C4−C9	1.060 *1.158*	1.062 *1.116*	1.062 *1.162*	1.044 *1.202*
		Amide Bond		
C14−O14	1.504 *1.454*	1.571 *1.512*	1.588 *1.516*	1.572 *1.513*
C14−N12	1.104 *1.173*	1.078 *1.130*	1.003 *1.107*	1.022 *1.121*
N12−C8	1.096 *1.050*	1.144 *1.076*	1.131 *1.068*	1.120 *1.064*

[a]Bond lengths (Å) and angles (degrees) for selected steps along the reaction coordinate. Standard deviations in parentheses.

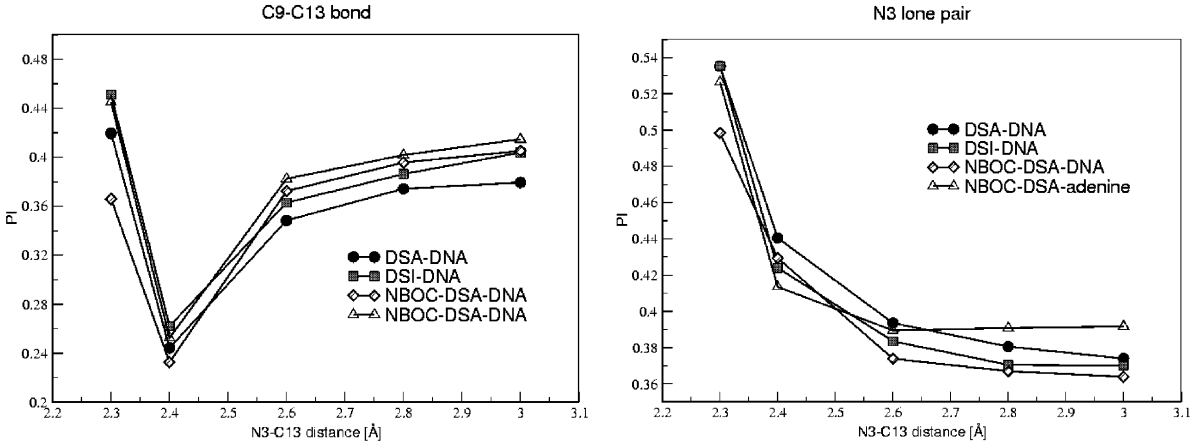

Figure 5. Hybrid Car−Parrinello QM/MM calculations. The electronic structure is investigated in terms of normalized Boys orbital centers, here defined as polarization index (PI). PIs representing the N3(A) electron lone pair and the C9−C13 chemical bond are shown for all four reactions investigated.

simulations of **DSA·DNA** and **DSI·DNA**, whereas they are found only at times in **NBOC−DSA·DNA** (see above).

For $3.3 < d < 2.8$ Å, the bond lengths of the cyclopropyl group decrease in the order, d(C9−C13) > d(C9−C10) > d(C10−C13), and the angles in the strained three-membered ring are close to 60°, as found experimentally in a structurally related compound (Cambridge database, RUGGAB[87]). This suggests that, in this range of d values, the structure of the reactive moiety of the drug is not significantly perturbed.

The C9−C13 bond is polarized toward C9 in the three complexes (the highest polarization in **DSA·DNA**, Table 2), while the N3 lone pair is polarized toward C13. The charge of N3 is slightly negative. The N3−C13 bond order is close to 0, thus no bond is detectable yet.

At d= 2.6 Å, the d(C9−C13) becomes slightly longer (by ∼0.01 Å) and more polarized toward C9 whereas the other two cyclopropyl bonds get shorter. No significant change is observed in the angles in the cyclopropyl unit. The N3 lone pair is more polarized (Figure 5), and its charge is slightly decreased (Table 2).

At d = 2.4 Å, the d(C9−C13) gets further elongated and the bond length fluctuates significantly (Table 2). The ∠(C13−C9−C10) and ∠(C10−C13−C9) angles are smaller than 50°, whereas ∠(C13−C10−C9) becomes as large as 87°.

At d = 2.3 Å, the constraint force is close to 0, and at the next step (d = 2.2 Å), the sign of the constraint force changes, indicating that the transition state has passed. Thus, we take the d = 2.3 Å as a model of the TS. d(C9−C13) is about 2.0 Å, d(C9−C10) is further shortened, and d(C10−C13) is slightly longer. ∠(C13−C9−C10) and ∠(C10−C13−C9) are significantly smaller than 60°, whereas ∠(C13−C10−C9) gets as large as 87°. The largest C13−C10−C9 angle is observed in **DSA·DNA**, which also features the longest C9−C13 bond.

The C9−C13 bond is strongly polarized toward C9, and the corresponding Boys orbital center resembles indeed more a lone pair localized on C9. This negative charge build-up at C9 can be stabilized by delocalization over the aromatic system of ring **A**, as seen in the change of bond lengths in the six-membered ring of the indole unit: d(C9−C8), d(C9−C4), d(C8−C7), and d(C6−C5) get shorter whereas d(C8−C7) and d(C5−C4) get longer. The changes in bond lengths are reflected in the bond orders (Table 2). The N3 lone pair is further polarized toward C13 (Figure 5), and the ESP charge is getting less and less negative. The decrease of negative charge on this center during the reaction illustrates qualitatively the charge transfer and tells about the proceeding of the reaction.[86] In **DSA·DNA**, the polarization of the N3 electron lone pair is the largest (Figure 5). The N3−C13 bond order increases along the reaction, but remains very small, whereas the C9−C13 bond order eventually becomes smaller than 0.5. The bond orders around the amide link also feel some variations during the reaction. The C14−O14 and N12−C8 bonds have slightly less double bond

TABLE 3: Electrostatic Calculations[a]

	NBOC−DSA·DNA		**NBOC−DSA·adenine**	
d(N3−C13) (Å)	3.3	3.0	3.3	3.0
C9	−6.65 (0.32)	−6.72 (0.22)	0.004 (0.047)	−0.11 (0.02)
C13	−7.62 (0.32)	−7.86 (0.24)	0.005 (0.050)	−0.27 (0.04)
D	0.97	1.14	∼0	0.16

[a] The electrostatic potentials on the C9 and C13 atoms of the drugs are reported (kT/e**)**. A constant dielectric constant for DNA and water and an even counterion distribution are assumed, results are here reported for qualitative comparisons. Potentials calculated for QM/MM calculation of **NBOC−DSA·DNA** and **NBOC−DSA·adenine**.

character at the transition state, whereas the bond order of the N12−C14 increases, suggesting a stronger conjugation with the indole unit.

Interestingly, during the QM/MM simulations, the χ_1 and χ_2 angle distribution of the noncovalent to the covalently bound drugs is similar to the classical one and almost as broad (Figure S6). The distribution does not change significantly along the reaction pathway (Table S5).

The calculated free energies are severely underestimated: their values range from 10.5 to 13.8 kcal/mol (Table 2), while the experimental ones (calculated from the quasi-first-order rate constants assuming Arrhenius behavior) range from 22 to 28 kcal/mol. The factors leading to such a large discrepancy between theory and experiment involve the accuracy of DFT and in particular the BLYP approximation for the exchange-correlation functional. The latter may underestimate the transition state energies. However, this does not seem to be the case for several chemical and enzymatic reactions[30,88] so far investigated with this method. In addition, calculations on a small test system, namely, *N*-acetyl cyclopropylindole with ammonia (Figure S2) with a different recipe for the exchange-correlation functional, the B3LYP, localized basis set (6-31G*), and implicit model of the solvent (PCM) (Table S6) provide calculated free energy, which is only 3 kcal/mol higher than the one calculated with BLYP and a delocalized basis set. Thus, the severe underestimation may be caused, at least in part, by the fact that DFT may describe poorly the highly delocalized exchange hole of S_N2 reactions' TS, where two electrons are delocalized over three atom centers.[43−46] A second factor involves the initial configuration used for the QM/MM simulations, in which the reactants are already in a favorable position. Because of the large flexibility of DNA,[13,14] the results might depend significantly on the conformation chosen. In addition, the location of the counterions may also affect the electronic structure.[89] We also neglect the energetic cost associated with the formation of the noncovalent complex. Since experiments are done under saturation condition,[6,15] this approximation should in principle be valid but could nevertheless lead to a further small error.[42] At least, we have chosen a simplified one-dimensional reaction coordinate, and we have limited the calculation of the energy profile to one long, constrained MD trajectory. For a more accurate estimate of the activation energy, several paths should be considered,[47,48] which was beyond our computational resources.

Reaction of NBOC−DSA with Adenine. As a reference reaction without the DNA scaffold, we chose the smallest compound **NBOC−DSA**, which is stable in water at pH 7.[90] The simulation is based on classical MD simulations of **NBOC−DSA·adenine**, in which *d* is constrained at 3.3 Å (see Methods). In the MD simulation, the N3(A) atom has no net solvation shell because of its vicinity to **NBOC−DSA**, whereas N1, which has a similar charge (−0.6 e), is fully solvated with two water molecules within 3.5 Å.

We follow the reaction using the same reaction coordinate as for the reaction toward **DNA**, analyzing the same steps along the reaction coordinate in terms of PI, bond orders, ESP charges, bond lengths, and angles (Table 2). In particular, ∠N3−C19−C9 can be taken as a measure for the ideal atom positioning for S_N2 reactions, in which the attacking and leaving groups are in-line and the central carbon atom adopts a trigonal bipyramidal structure. This angle varies significantly during the reaction. Instead, in the reaction of **NBOC−DSA·DNA**, the ∠N3−C19−C9 angle changes very little (from 157−170°) because of geometrical constraints. We focus now on the difference between the two reactions.

At $d = 3.0$ Å, the C9−C13 bond is less polarized in **NBOC−DSA·adenine** (Figure 5), suggesting that this polarization is a key feature for the increase in reactivity of the drug caused by **DNA**. Poisson−Boltzmann calculations at the C9 and C13 sites (Table 3) show as expected that, in **DNA**, the electrostatic potential is highly negative and furthermore more negative at the C9 position than at the C13 position. In water, the electrostatic potential is close to zero. Even though the bond orders at this stage of the reaction are very similar (Table 2), the D-RESP charges are more negative and the N3 lone pair of adenine more polarized in **NBOC−DSA·adenine** (Table 2).

In the following at $d = 2.8$, 2.6, and 2.4 Å, the polarization of this electron lone pair remains almost constant in **NBOC−DSA·adenine** whereas it increases in **NBOC−DSA·DNA**, and at $d = 2.4$ Å, the polarization of N3 toward C13 is very similar in both reactions. *d*(C9−C13) undergoes similar changes in both environments and increases steadily, whereas the ∠(C13−C9−C10) and ∠(C10−C13−C9) angles decrease, ∠(C13−C10−C9) increases, and the absolute values compare very well.

At $d = 2.3$ Å, *d*(C9−C13) is around 2 Å and longer in **NBOC−DSA·adenine** than in **NBOC−DSA·DNA**. In both reactions, the N3 lone pair is largely polarized toward C13, indicating the formation of a bond between these two atom centers. The bond orders are still rather small but indicate the formation of the bond. The C9−C13 bond order is larger in DNA than in water, whereas the N3−C13 bond order is smaller (Table 2). Thus, both bond formation and bond breakage are less advanced in the DNA environment compared to the reaction in water, pointing to an earlier TS. In general, an early transition is associated with a low activation barrier. In agreement with this general rule, we find that the activation barrier for the reaction in DNA is 4 kcal/mol lower than the one in water (Table 2). On the other hand, from inspection of the torsions and bond orders around the vinylogous bonds, no striking differences are found between the two reactions (Table 2). The D-RESP charges on N3 become less negative during both reactions but more so in the reaction in DNA (Table 2).

V. Discussion

We have presented a theoretical investigation of the key steps of the binding of duocarmycins to the d(pGpApCpTpA-pApTpTpGpApC)-d(pGpTpCpApApTpTpA*pGpTpC) oligonucleotide (**DNA**).

Classical MD simulations on the 10 ns time scale have provided the mode of binding of noncovalent complexes (i.e., before the reaction takes place) between the **DSA**, **DSI**, and **NBOC−DSA** and **DNA**. The accuracy of our computational setup has been established by comparing MD simulations of the covalent adduct with NMR data. All the parameters with the exception of the χ_1 angle for **DSA·DNA** compare very well with experiment (Table 1). As for χ_1, although its MD average value for **DSA·DNA** is smaller by 7° relative to the NMR structure, the *distribution* of the χ_1 values is rather broad and overlaps with the NMR value. We conclude that our MD setup describes rather accurately duocarmycins/DNA interactions.

Our MD simulations on the noncovalent adduct suggest that **NBOC−DSA** binds less tightly than **DSA** and **DSI** to **DNA** because of the presence of the *tert*-butyl unit, which is shorter and bulkier than the indole unit of the other two drugs (Figure 1). The *tert*-butyl unit penetrates therefore less into the minor groove, and the interactions also involve fewer DNA residues. As a result, reactive conformations, in which the cyclopropyl moiety of the drug is in close contact (about 3 Å) with the reactive adenine nucleobase, are frequently encountered for only **DSA** and **DSI**. In addition, **NBOC−DSA** binds rather unspecifically to **DNA** relative to the other two, as the drug cyclopropyl interacts with N3(G20) as well.

The structures of all the DNA systems investigated here are similar and differ substantially from that of B-DNA, as expected for an A-tract-containing oligonucleotide.[9−11] The drugs bind to **DNA** by removing two to three ordered water molecules (occupancy <20%, Figure 4). Formation of the covalent adduct causes the removal of a further number of water molecules (5 to 6 fully dehydrated sites).

The large-scale motions of all the models investigated here involve the bending of the entire DNA double helix and the opening and closing of the DNA minor groove. The latter motion is slightly larger in the noncovalent complexes than in **DNA**, and it is much smaller in the covalent ones (Figure S4/S5). The different mobilities of covalent and noncovalent complexes might be relevant for molecular recognition processes and the drug/DNA reactivity.

The DNA structure is not greatly affected by drug binding. Thus, we expect that in the binding process a free energy cost is associated to DNA dehydration (counterbalanced by the free energy of drug binding), while that associated to conformational changes of the DNA scaffold is probably less significant. The drugs' conformation changes when passing from the noncovalent to the covalent adducts. The torsional angles χ_1 (C7−C8−N12−C16) and χ_2 (C8−N12−C16−O16) are used to describe the conformational properties. In the noncovalent adducts, the average χ_1 and χ_2 angles in **DSA** and **DSI** are very similar and larger than those in **NBOC−DSA**. In the corresponding covalent drug−DNA adducts, the average χ_1 is smaller and the standard deviations are also much lower. Thus, the drug is more flexible and distorted in the noncovalent than in the covalent complex. In the covalent complexes, the smaller minor groove width relative to the free oligonucleotide, along with the relative rigidity of the entire complexes might play a role for their interaction with the duocarmycin−DNA adduct recognizing protein, DARP.[91] On the other hand, the relatively large fluctuations of the noncovalent complex could help to trap the DNA in a reactive conformation, as suggested by ref 19. The χ_1 and χ_2 values of the noncovalent complexes differ by only few degrees in our simulation but exhibit large standard deviations. This observation might suggest that the "shape induced activation" mechanism, in which the differences between such angles does not play a crucial role for the alkylation.[4,6]

Our investigation has been complemented by hybrid Car−Parrinello/MM simulations[63,66] of the rate-limiting, first step of the alkylation reactions performed by the drugs. The calculations are based on reactive conformations of the noncovalent drug−DNA structures, in which the drugs are in a favorable orientation and in close contact with the oligonucleotide for the S_N2 reaction. These are frequently found in the MD simulations of **DSA·DNA** and **DSI·DNA** (Table 1), whereas they are found only at times in **NBOC−DSA·DNA**. Thus, **DSA** and **DSI** have an optimal interaction with the DNA scaffold.

The activation free energies are calculated using thermodynamic integration along the *d*(N3(A)−C13(drug)) reaction coordinate. These are rather alike for all three drugs and severely underestimated relative to the experimental values. The factors leading to such a large discrepancy between theory and experiment involve, at least in part, the accuracy of DFT and the choice of the starting configurations, as outlined in the Introduction and Results sections. Within the approximation of the protocol adopted here, we follow the structural and electronic properties of the alkylation reaction. During the reaction, the C9−C13 bond of the cyclopropyl unit gets progressively longer and more polarized toward C9, while the other two bonds in the three-membered rings get slightly shorter. The N3(A19) electron lone pair becomes more polarized toward C13, and the negative charge at N3 slowly decreases until it eventually becomes positive at the transition state. At the transition state, the C9−C13 bond is broken (Table 2) and the corresponding electron pair is mainly localized on C9. The negative charge build-up at this center can be efficiently stabilized by delocalization over the aromatic system. As a result, the delocalization in the ring system is augmented (Table 2) following the scheme in Figure 1 closely. The bond orders of the six-membered ring are progressively changing toward similar values. The distribution of the torsional angles χ_1 and χ_2 in **DSA** and **DSI** compare fairly well, and the average values are slightly larger than in **NBOC−DSA** (Table 1). They are similar with the classical MD simulation. Comparison with the corresponding reaction in water for the smaller of these drugs, **NBOC−DSA**, provides valuable insights on the effect of the DNA scaffold on its reactivity. **NBOC−DSA** reacts with DNA but is stable at pH 7 toward adenine. We find that (i) the C9−C13 bond is more polarized in DNA than in water in the beginning of the reaction, (ii) N3 of adenine is less negative in DNA than in water, which could render the charge transfer more easy in DNA, and (iii) the bond orders at the transition state show that in DNA the system is more reactant-like than in water (Table 2). An early transition state is usually characterized by a low activation barrier. All these points are in agreement with the observed activation free energy, which is 4 kcal/mol larger in water than in DNA. This corresponds to a rate acceleration of roughly 3 orders of magnitude. Thus, although the activation free energy of the model reaction is also smaller than the experimental data, our calculations are qualitatively in agreement with experiment, in that the DNA frame accelerates the reaction rate. On the other hand, a conformational change in the DNA or the drug seems to be less relevant to the rate of acceleration.

Note Added in Proof: A recent DFT study suggests that the acid catalysis under physiological conditions, not considered in the present investigation, plays a minor role for the DNA alkylation (Freccero, M.; Gandolfi, R. *J. Org. Chem.* **2005**, *70*, 7098−7106).

Acknowledgment. We thank Simone Raugei and Alessandra Magistrato for useful discussions. This project was financed by INFM and COFIN-MURST. CINECA supercomputing center is also acknowledged for support.

Supporting Information Available: Figures containing (i) superposition of NMR structure and covalent DSA−DNA MD average structure, (ii) schematic figure of test system *N*-acetyl cyclopropylindole with ammonia, (iii) selected rmsd of classical MD and drug−adenine distances, (iv) changes in the minor groove width along the first three normal modes, (v) changes in the local axis bend along normal modes, and (vi) torsional angle distributions. Tables in Supporting Information contain (i) geometry optimization of the DSA model compound in vacuo with changing torsional angles, (ii−iv) selected DNA structure parameters with standard deviations, (v) torsional angles along QM/MM trajectories, and (vi) test calculations on *N*-acetyl cyclopropylindole at the B3LYP and BLYP levels of theory. This material is available free of charge via the Internet at http://pubs.acs.org.

References and Notes

(1) Eis, P. S.; Smith, J. A.; Rydzewski, J. M.; Case, D. A.; Boger, D. L.; Chazin, W. J. *J. Mol. Biol.* **1997**, *272*, 237−252.
(2) Lin, C. H.; Patel, D. J. *J. Mol. Biol.* **1995**, *248*, 162−179.
(3) Yasuzawa, T.; Muroi, K.; Ichimura, M.; Takahashi, I.; Ogawa, T.; Takahashi, K.; Sano, H.; Saitoh, Y. *Chem. Pharm. Bull.* **1995**, *43*, 378.
(4) Boger, D. L.; Garbaccio, R. M. *Acc. Chem. Res.* **1999**, *32*, 1043−1052.
(5) Small, E. J.; Figlin, R.; Petrylak, D.; Vaughn, D. J.; Sartor, O.; Horak, I.; Pincus, R.; Kremer, A.; Bowden, C. *Invest. New Drugs* **2000**, *18*, 193−197.
(6) Boger, D. L.; Garbaccio, R. M. *Bioorg. Med. Chem.* **1997**, *5* (2), 263−276.
(7) Cimino, P.; Improta, R.; Bifulco, G.; Riccio, R.; Gomez-Paloma, L.; Barone, V. *J. Org. Chem.* **2004**, *69*, 2816−2824.
(8) Schnell, J. R.; Ketchem, R. R.; Boger, D. L.; Chazin, W. J. *J. Am. Chem. Soc.* **1999**, *121*, 5645−5652.
(9) Katahira, M.; Sugeta, H.; Kyogoku, Y. *Nucleic Acids Res.* **1990**, *18*, 613−618.
(10) Nadeau, J. G.; Crothers, D. M. *Proc. Natl. Acad. Sci. U.S.A.* **1989**, *86*, 2622−2626.
(11) Haran, T. E.; Crothers, D. M. *Biochemistry* **1989**, *28*, 2763−2767.
(12) Madhumalar, A.; Bansal, M. *Biophys. J.* **2003**, *85*, 1805−1816.
(13) Beveridge, D. L.; Dixit, S. B.; Barreiro, G.; Thayer, K. M. *Biopolymers* **2004**, *73*, 380−403.
(14) Mack, D. R.; Chiu, T. K.; Dickerson, R. E. *Biochemistry* **2001**, *312*, 1037−1049.
(15) Boger, D. L.; Hertzog, D. L.; Bollinger, B.; Johnson, D. S.; Cai, H.; Goldberg, J.; Turnbull, P. *J. Am. Chem. Soc.* **1997**, *119*, 4977−4986.
(16) Boger, D. L.; Bollinger, B.; Hertzog, D. L.; Johnson, D. S.; Cai, H.; Mesini, P.; Garbaccio, R. M.; Jin, Q.; Kitos, P. A. *J. Am. Chem. Soc.* **1997**, *119*, 4987−4998.
(17) Hurley, L. H.; Lee, Ch.-S.; McGovren, J. P.; Warpehoski, M. A.; Mitchell, M. A.; Kelly, R. C.; Aristoff, P. A. *Biochemistry* **1988**, *27*, 3886−3892.
(18) Sun, D.; Lin, C. H.; Hurley, L. H. *Biochemistry* **1993**, *32*, 4487−4495.
(19) (a) Thompson, A. S.; Sun, D.; Hurley, L. H. *J. Am. Chem. Soc.* **1995**, *117*, 2371−2372. (b) Freccero, M.; Gandolfi, R. *J. Org. Chem.* **2004**, *69*, 6202−6213.
(20) Kirschner, K. N.; Lee, M.; Stanley, R. C.; Bowen, J. P. *Bioorg. Med. Chem.* **2000**, *8*, 329−335.
(21) Lamm, G.; Wong, L.; Pack, G. R. *J. Am. Chem. Soc.* **1996**, *118* (14), 3325−3331.
(22) Warpehoski, M. A.; Harper, D. E. *J. Am. Chem. Soc.* **1994**, *116*, 7573−7580.
(23) Jayaram, B.; Sharp, K. A.; Honig, B. *Biopolymers* **1989**, *28*, 975−993.
(24) Lamm, G.; Pack, G. R. *Proc. Natl. Acad. Sci. U.S.A.* **1990**, *87*, 9033−9036.
(25) Ambroise, Y.; Boger, D. L. *Bioorg. Med. Chem. Lett.* **2002**, *12*, 303.
(26) Boger, D.; Garbaccio, R. M. *J. Org. Chem.* **1999**, *64* (15), 5666−5669.
(27) Case, D. A.; Pearlman, D. A.; Caldwell, J. W.; Cheatham, T. E., III; Ross, W. S.; Simmerling, C. L.; Darden, T. A.; Merz, K. M.; Stanton, R. V.; Cheng, A. L.; Vincent, J. J.; Crowley, M.; Tsui, V.; Radner, R. J.; Duan, Y.; Pitera, J.; Massova, I.; Seibel, G. L.; Singh, U. C.; Weiner, P. K.; Kollman, P. A. *AMBER6*; University of California: San Francisco, CA, 1999.
(28) Cheatham, T. E., III; Cieplak, P.; Kollman, P. A. *J. Biomol. Struct. Dyn.* **1999**, *16*, 845−862.
(29) Pearlman, D. A.; Case, D. A.; Caldwell, J. W.; Ross, W. S.; Cheatham, T. E., III; DeBolt, S.; Ferguson, D.; Seibel, G. L.; Kollman, P. A. *Comput. Phys. Commun.* **1995**, *91*, 1−41.
(30) Sulpizi, M.; Laio, A.; VandeVondele, J.; Cattaneo, A.; Rothlisberger, U.; Carloni, P. *Proteins* **2003**, *52* (2), 212−224.
(31) Becke, A. D. *Phys. Rev. A* **1988**, *38*, 3098−3100.
(32) Lee, C.; Yang, W.; Parr, R. G. *Phys. Rev. B* **1988**, *37*, 785−789.
(33) Rothlisberger, U. 15 Years of Car−Parrinello Simulations in Physics, Chemistry and Biology. In *Computational Chemistry: Reviews of Current Trends*; Leszczynski, J., Ed.; World Scientific: 2001; Vol. 6, pp 33−68.
(34) Dal Peraro, M.; Llarrull, L. I.; Rothlisberger, U.; Vila, A. J.; Carloni, P. *J. Am. Chem. Soc.* **2004**, *126* (39), 12661−12668.
(35) Guidoni, L.; Spiegel, K.; Zumstein, M.; Roethlisberger, U. *Angew. Chem.* **2004**, *116*, 3348−3351.
(36) Schlegel, H. B. *J. Comput. Chem.* **2003**, *24* (12), 1514−1527.
(37) Stubbs, J. M.; Marx, D. *J. Am. Chem. Soc.* **2003**, *125* (36), 10960−10962.
(38) Kirchner, B.; Reiher, M.; Hille, A.; Hutter, J.; Hess, B. A. *Chemistry* **2005**, *11* (2), 574−583.
(39) Semialjac, M.; Schroder, D.; Schwarz, H. *Chemistry* **2003**, *9* (18), 4396−4404.
(40) Stirling, A.; Iannuzzi, M.; Laio, A.; Parrinello, M. *Chem. Phys. Chem.* **2004**, *5* (10), 1558−1568.
(41) De Vivo, M.; Ensing, B.; Klein, M. L. *J. Am. Chem. Soc.* **2005**, *127* (32), 11226−11227.
(42) Tidor, B.; Karplus, M. *J. Mol. Biol.* **1995**, *238*, 405−414.
(43) Ensing, B.; Meijer, E. J.; Blöchl, P. E.; Baerends, E.-J. *J. Phys. Chem. A* **2001**, *105*, 3300−3310.
(44) Gritsenko, O. V.; Ensing, B.; Schipper, P. R. T.; Baerends, E.-J. *J. Phys. Chem. A* **2000**, *104*, 8558−8565.
(45) Lynch, B. J.; Truhlar, D. G. *J. Phys. Chem. A* **2001**, *105*, 2936−2941.
(46) Raugei, S.; Cardini, G.; Schettino, V. *J. Chem. Phys.* **1999**, *24*, 10887−10894.
(47) Dellago, C.; Bolhuis, P. G.; Chandler, D. *J. Chem. Phys.* **1999**, *110* (14), 6617−6625.
(48) Gregersen, B. A.; Lopez, X.; York, D. M. *J. Am. Chem. Soc.* **2003**, *126*, 7504−7513.
(49) Laio, A.; Parrinello, M. *Proc. Natl. Acad. Sci. U.S.A.* **2002**, *99*, 12562−12566.
(50) Cornell, W. D.; Cieplak, P.; Bayly, C. I.; Gould, I. R.; Merz, K. M., Jr.; Ferguson, D. M.; Spellmeyer, D. C.; Fox, T.; Caldwell, J. W.; Kollman, P. A. *J. Chem. Phys.* **1995**, *117*, 5179−5197.
(51) Jorgensen, W. L.; Chandrasekhar, J.; Madura, J. D.; Impey, R. W.; Klein, M. L. *J. Chem. Phys.* **1983**, *79* (2), 926−935.
(52) Aaqvist, J. *J. Phys. Chem.* **1990**, *94*, 8021−8024.
(53) Wang, J.; Wolf, R. M.; Caldwell, J. W.; Kollman, P. A. *J. Comput.Chem.* **2004**, *25*, 1157−1174.
(54) Nosé, S. J. *J. Chem. Phys.* **1984**, *81*, 511−519.
(55) Hoover, W. G. *Phys. Rev. A* **1985**, *31*, 1695−1697.
(56) Nosé, S. J. *Mol. Phys.* **1984**, *52*, 255.
(57) Parrinello, M.; Rahman, A. *J. Appl. Phys.* **1981**, *52*, 7182−7190.
(58) Leach, A. *Molecular Modelling: Principles and Applications*; Addison-Wesley Longman: Essex, U.K., 1996.
(59) Swaminathan, S.; Ravishanker, G.; Beveridge, D. L.; Lavery, R.; Etchebest, C.; Sklenar, H. *Proteins* **1990**, *8* (2), 179−193.
(60) Hess, B. *Phys. Rev. E.* **2000**, *62* (6), 8438−8448.
(61) Hess, B. *Phys. Rev. E.* **2002**, *65*, 031910−1−031910−9.
(62) van der Spoel, D.; van Buuren, A. R.; Apol, E.; Meulenhoff, P. J.; Tieleman, D. P.; Sijbers, A. L. T. M.; Hess, B.; Feenstra, K. A.; Lindahl, E.; van Drunden, R.; Berendsen, H. J. C. *Gromacs User Manual*, version 3.1.1; Nijenborgh 4, 9747 Groningen, The Netherlands, 2002.
(63) Hutter, J.; Alavi, A.; Deutsch, T.; Silvestri, W.; Parrinello, M.; Rothlisberger, U.; Marx, D.; Focher, P.; Tuckerman, M.; Andreoni, W.; Curioni, A.; Fois, E.; Giannozzi, P.; Sebastiani, D.; Laio, A.; VandeVondele, J.; Seitsonen, A.; Billeter, S. *CPMD.MPI fuer Festkoerperforschung Stuttgard and IBM Zurich Research Laboratory (3.4.)*, 2000.
(64) Troullier, N.; Martins, J. L. *Phys. Rev. B* **1991**, *43*, 1943−2006.
(65) Barnett, R. N.; Landman, U. *Phys. Rev. B* **1993**, *48*, 2081−2097.
(66) Laio, A.; VandeVondele, J.; Rothlisberger, U. *J. Chem. Phys.* **2002**, *116*, 6941.
(67) Sebastiani, D.; Rothlisberger, U. Advances in Density-functional-based Modeling Techniques—Recent Extensions of the Car−Parrinello

Approach, In *Quantum Medicinal Chemistry*, 1 ed.; Carloni, P., Alber, F., Eds.; Wiley-VCH: Weinheim, Germany, 2003; Chapter 1, pp 5−36.
(68) Carter, E. A.; Ciccotti, G.; Hynes, J. T.; Kapral, R. *Chem. Phys. Lett.* **1989**, *156*, 472.
(69) Ivanov, I.; Klein, M. L. *J. Am. Chem. Soc.* **2002**, *124*, 13380−13381.
(70) Carter, E. A.; Ciccotti, G.; Hynes, J. T.; Kapral, R. *Chem. Phys. Lett.* **1989**, *156* (5), 472−477.
(71) Ciccotti, G.; Ferrario, M. *J. Mol. Liq.* **2000**, *89* (1−3), 1−18.
(72) Sprik, M.; Ciccotti, G. *J. Chem. Phys.* **1998**, *109* (18), 7737−7744.
(73) Finkelstein, A. V.; Ptitsyn, O. B. *Protein Physics: A Course of Lectures;* 1 ed.; Academic: New York, 2002.
(74) Marzari, N.; Vanderbilt, D. *Phys. Rev. B* **1997**, *56*, 12847−12865.
(75) Alber, F.; Folkers, G.; Carloni, P. *J. Phys. Chem. B* **1999**, *103*, 6121−6126.
(76) De Proft, F.; Van Alsenoy, C.; Peeters, A.; Langenaeker, W.; Geerlings, P. *J. Comput. Chem.* **2002**, *23* (12), 1198−1209.
(77) Mayer, I. *Int. J. Quantum Chem.* **1986**, *29*, 73.
(78) Rocchia, W.; Alexov, E.; Honig, B. *J. Phys. Chem. B* **2001**, *105* (28), 6507−6514.
(79) Gilson, M. K.; Sharp, K.; Honig, B. *J. Comput.Chem.* **1987**, *9*, 327−335.
(80) Honig, B.; Nicholls, A. *Science* **1995**, *268* (5214), 1144−1149.
(81) Pack, G. R.; Garrett, G. A.; Wong, L.; Lamm, G. *Biophys. J.* **1993**, *65*, 1363−1370.
(82) Blackburn, G. M.; Gait, M. J. *Nucleic Acids in Chemistry and Biology.;* Oxford Universtiy Press: Oxford, U.K., 1996.
(83) Boger, D. L.; Johnson, D. S.; Yun, W. *J. Am. Chem. Soc.* **1994**, *116*, 1635−1656.
(84) Beveridge, D. L.; McConnell, K. J. *Curr. Opin. Struct. Biol.* **2000**, *10*, 182−196.
(85) Boger, D. L.; Goldberg, J.; McKie, J. A. *Bioorg. Med. Chem. Lett.* **1996**, *6*, 1955−1960.
(86) Laio, A.; VandeVondele, J.; Rothlisberger, U. *J. Phys. Chem. B* **2002**, *106*, 7300−7307.
(87) Parrish, J. P.; Kastrinsky, D. B.; Boger, D. L. *Org. Lett.* **2003**, *5* (14), 2577−2579.
(88) Magistrato, A.; Maurer, P.; Fassler, T.; Rothlisberger, U. *J. Phys. Chem. A* **2004**, *108*, 2008−2013.
(89) Barnett, R. N.; Cleveland, C. L.; Joy, A.; Landman, U.; Schuster, G. B. *Science* **2001**, *294*, 567−571.
(90) Boger, D. L.; Kozo, M.; Hertzog, D. L.; Kitos, P. A.; Holmes, D. *J. Am. Chem. Soc.* **1993**, *115*, 9025−9036.
(91) Asai, A.; Yano, K.; Mizukami, T.; Nakano, H. *Cancer Res.* **1999**, *59*, 5417−5420.